SOUNDING THE TROPOSPHERE FROM SPACE: A NEW ERA FOR GLOBAL ATMOSPHERIC CHEMISTRY

ALEXANDER KOKHANOVSKY, JOHN P. BURROWS, HEINRICH BOVENSMANN, MICHAEL BUCHWITZ, ANNETTE LADSTÄTTER-WEIβENMAYER, STEFAN NOËL, ANDREAS RICHTER, VLADMIR ROZANOV, WOLFGANG VON HOYNINGEN-HUENE, MARK WEBER

Institute of Environmental Physics, University of Bremen,
O. Hahn Allee 1, D-28334 Bremen, Germany

Abstract The purpose of this paper is to give an overview of the state-of-art in the field of retrieval of total vertical columns of trace gases from spaceborne observations. Most retrievals presented in the paper are based on the hyperspectral measurements of the Global Ozone Monitoring Experiment (GOME) and the SCanning Imaging Absorption SpectroMeter for Atmospheric CHartographY (SCIAMACHY). Both GOME and SCIMACHY are currently orbiting the planet and providing a wealth of information on the Earth'satmosphere. In particular, the retrieval of vertical columns of following trace gases are discussed: CO, CO_2, CH_4, O_3, NO_2, SO_2, and H_2O. In addition, the technique to retrieve the particulate matter concentration using satellite measurements is described.

1. Introduction

The atmospheric air is composed mainly of of molecular nitrogen, molecular oxygen and argon. The total volume mixing ratio of all other atmospheric gases is just around 0.1% for dry air. Therefore, they are called the trace gases. Although the total vertical columns (VC) of these gases are very small, trace gases have a profound influence on atmospheric chemistry, pollution, and climate. This influence has a global nature and, therefore, studies of the chemical composition of the atmosphere must be global as well. This can be done only using satellite measurements. In particular, spectrometers on geostationary orbits will provide the required information on the atmospheric chemical composition with high temporal and spatial resolution necessary for the improvement of chemical atmospheric models and various climate scenarios, and also for forecasts of pollution levels and trajectories.

Currently, instruments for monitoring of trace gas vertical columns are not available at geostationary satellites although up-to-date technology permits the deployment and operation of such instruments. Clearly, such measurements will be

available in the nearest future. Present atmospheric chemistry missions operate from polar orbiting satellites. This includes among others (see, e.g., Gottwald et al. (2006) for more details on past and present atmospheric chemistry missions) the Global Ozone Monitoring Experiment (GOME-1) on board ESA's ERS-2 satellite (launch date: April 21st, 1995), The SCanning Imaging Absorption SpectroMeter for Atmospheric CHartographY (SCIAMACHY) onboard ESA's ENVIronmental SATellite (ENVISAT) (launch date: March 1st, 2002), the Ozone Monitoring Instrument (OMI) on board NASA's EOS-AURA satellite (launch date: July 15th, 2004), and the Global Ozone Monitoring Experiment (GOME-2) onboard EUMETSAT present and future MetOp 1, 2, and 3 platforms (2006-2020). The characteristic feature of all these instruments is the capability to perform hyperspectral measurements. The spectral resolution of SCIAMACHY depends on the spectral region and is in the range 0.24-1.48nm. Measurements cover the broad range of wavelengths from 240 to 2380nm at about 8000 individual wavelength bins. The spectral resolution of GOME-1 is 0.2-0.33nm in the spectral range 240-790nm. OMI has the spectral resolution 0.45-1 nm in the spectral region 270-500nm.

The high spectral resolution is needed because measurements of trace gas vertical columns are based on the principles of the Differential Optical Absorption Spectroscopy (DOAS) (Platt and Stutz, 2008). Traditional ground – based DOAS instrumentation operates on a well-established scientific principle, Beer-Lambert's absorption law, which relates the quantity of light absorbed to the number of gas molecules in the light path. The application of DOAS to satellite measurements is somewhat involved because it requires an accurate modeling of multiply scattered light before it reaches the satellite instrument. The modeling is based on radiative transfer principles (Chandrasekhar, 1960). Usually smoothly varying signal is subtracted from the observed spectral curves of top-of-atmosphere (TOA) reflectances R and the depth of various gaseous absorption bands is analyzed. The subtraction of the smoothly varying signals enables partial account for *a priori* unknown properties of atmospheric and surface multiple light scattering effects. Clearly, deeper absorption bands also mean larger trace gas vertical columns. The inversion procedure is based on the minimization of the function

$$f(V) = \left\| R_{mes}(\lambda,V) - R_{calc}(\lambda,V) \right\|^2 \qquad (1)$$

with respect to the vertical column of a given trace gas V for a selected range of wavelengths λ. Here $R_{mes(calc)}$ is the measured (calculated) spectral TOA reflectance. The details of the numerical procedures are discussed, e.g., by Rozanov et al. (1998) and Buchwitz et al. (2000). The procedures account for the influence of light scattering by ground surface and aerosols. Cloud screening and cloud characterization algorithms are applied before the trace gas retrievals are performed (Kokhanovsky, 2007a,b). The most accurate results are obtained for clear sky conditions. Although there is also a weak sensitivity of the signal detected on a satellite to the tropospheric trace gas abundances under the clouds for the cases of thin clouds. However, in most cases the tropospheric vertical columns of trace gases under the clouds can not be retrieved due to the cloud shielding effects.

Clouds can be accounted for in the retrieval of vertical columns of trace gases, which have maximal concentrations in the stratosphere (e.g., ozone). Usually a broken

cloud field is modeled in the framework of the independent pixel approximation assuming that

$$R_{calc} = cR_c + (1-c)R_a \,, \tag{2}$$

where c is the cloud fraction in the pixel studied, R_c is the cloud reflectance, R_a is the clear sky reflectance. The accuracy of this approximation for the satellite ozone retrievals was studied by Kokhanovsky et al. (2007a) using 3-D Monte-Carlo calculations. An important parameter for trace gas retrievals in cloudy conditions is the cloud top height, which can be retrieved from measurements in the oxygen A-band located at 760nm. High clouds screen more oxygen thereby reducing the depth of the oxygen A-band, clearly seen in the TOA reflectance spectra. This effect is used for the cloud top height monitoring from a satellite (Kokhanovsky et al., 2007b).

The main task of this paper is to give an overview of the results obtained with respect to the trace gas monitoring from space using GOME and SCIAMACHY. A short description of these advanced satellite spectrometers is given in the next section. Selected retrieval results are presented in Section 3. Section 4 is aimed to aerosol remote sensing from space.

2. Satellite instruments

2.1. GOME

GOME-1 is a passive imaging spectrometer providing high spectral resolution. It was launched in April 1995 on the ERS-2 satellite and marks the beginning of a long-term European ozone monitoring effort. Scientists receive from this experiment high quality data on the global distribution of ozone and several other relevant trace gases such as BrO, OClO and NO_2 in the Earth's atmosphere. GOME is a nadir-sounding instrument looking down on the Earth's surface. The spectrometer operates in the ultraviolet and visible spectral range (240 - 790 nm). The spectral resolution is excellent. It is in the range 2.0-3.3Å, depending on frequency. Depending on the measurement mode, GOME provides a horizontal resolution from 40 km along track and 320 km across track to 40 km along track and 40 km across track. Measurements are performed in four channels.

GOME data products are divided into different levels depending on the processing step. Level 0 data are the raw data as they are down-linked to the ground-stations. In a first step, raw data are converted into radiances using information from calibration measurements (Level 1). In a second step, a radiative transfer model and retrieval process are applied to convert the radiances into trace gas concentrations. Level 2 data, therefore, contain footprints of trace gas concentrations along the satellite's orbit. Level 3 data are geophysical parameters that have been spatially (e.g., $1°$ averages) and/or temporally (e.g., yearly means) resampled from Level 1 or Level 2 data. Level 4 data are outputs or results from models (e.g., assimilation) using lower level data as inputs and, thus, not directly derived from the instruments.

GOME-2 is an improved version of GOME-1 currently operating onboard EUMETSAT MetOp-1 platform. The four main channels provide continuous spectral coverage of the wavelengths between 240 and 790nm with the spectral resolution 2.6-5.1 Å. The instrument has in addition two polarization channels in the range 300-800nm with 15 programmable bands. The spatial resolution is 80⊔40km².

2.2. SCIAMACHY

SCIAMACHY is a passive imaging spectrometer, comprising a mirror system, a telescope, a spectrometer, and thermal and electronic subsystems. The full resolution spectral information is generated in 8 science channels (see Table 1). The possibility to retrieve the vertical column of a given trace gas depends on the wavelength range used.

The correspondence of channels and various trace gas concentrations retrieved in a given channel is shown in Table 1. The radiation corresponding to channel 1 hardly penetrates to the lower troposphere due to strong gaseous absorption. Therefore, it is used exclusively for stratospheric and mesospheric studies (Gottwald et al., 2006).

SCIAMACHY has a capability to retrieve the vertical profiles of selected trace gases using the limb observation mode. The limb mode enhances the SCIAMACHY performance. However, this also leads to the fact that half of the nadir data is missing because SCIAMACHY looks in limb and not in the nadir for the half time of the entire mission. The spatial resolution of SCIAMACHY varies depending on the location of measurements and also on the channel. It is usually 30km $\times$ 60km which is better than for GOME but large compared to the typical size of a city. This relatively poor resolution is due to the fact that the trace gas concentrations are usually low and, therefore, one must observe a relatively large area to have a good signal-to-noise ratio. Also there are limitations with respect to the possible amount of information which can be downloaded from a satellite daily. The swath of SCIAMACHY is 960km and one SCIAMACHY state covers a large region with the size of 390km $\times$ 960km. SCIAMACHY nadir states are separated by areas, where no nadir measurements are performed because of limb observations.

An interesting aspect of SCIAMACHY is the possibility to get information on the variability of reflectance in the SCIAMACHY science pixel using the polarization Measurement Devices (PMDs). The spatial resolution of PMDs is usually 7.5km $\times$ 30km. Therefore, one typically finds 8 PMD measurements in one SCIAMACHY pixel. This is used, e.g., for SCIAMACHY cloud screening algorithms. PMDs measure light polarized perpendicular to the SCIAMACHY optical plane, generated by a Brewster angle reflection at the second face of the pre-dispersing prism. The polarized beam is split into 6 different spectral bands (see Table 2). The seventh PMD channel measures the $45°$ component of the light extracted from the channels 3-6 light paths. PMDs are needed to asses the measurement sensitivity of the spectrometer depending on the polarization state of the incoming light beam. They are used in GOME as well (Burrows et al., 1999).

Table 1. SCIAMACHY science channels (Gottwald et al., 2006) and vertical columns of trace gases, which have absorption bands in correspondent channels.

Channel	Spectral range(nm)	Resolution (nm)	Vertical columns
1	214-334	0.24	O_3
2	300-412	0.26	O_3, BrO, OClO, HCHO, SO_2
3	383-628	0.44	NO_2, CHOCHO, IO
4	595-812	0.48	H_2O, O_2
5	773-1063	0.54	H_2O
6	971-1773	1.48	CH_4, CO_2, H_2O
7	1934-2044	0.22	CO_2, H_2O
8	2259-2386	0.26	CO, CH_4, N_2O, H_2O

Table 2. SCIAMACHY PMDs.

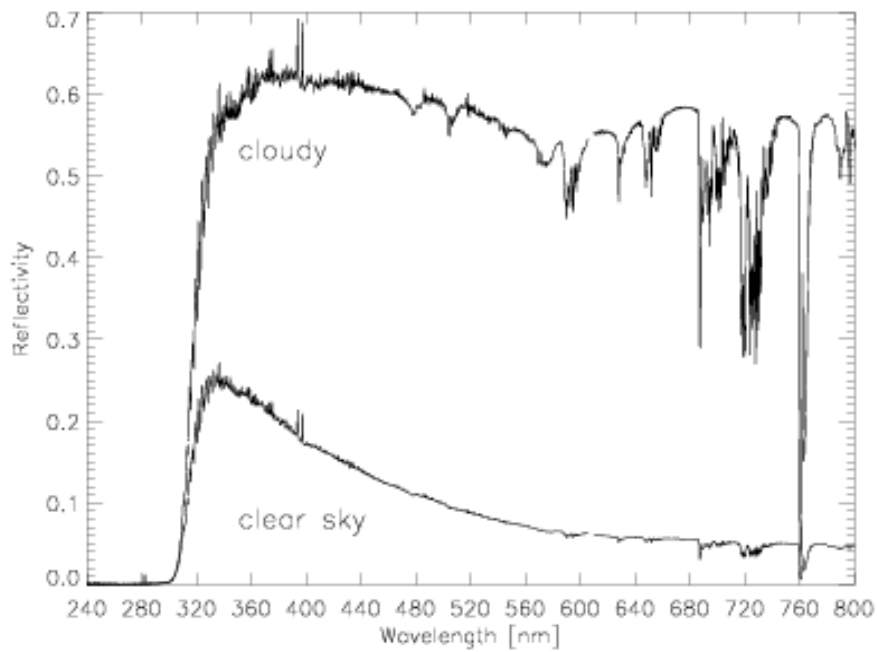| PMD	Spectral range, nm	Spectral band width, nm
1	310-365	55
2	455-515	60
3	610-690	80
4	800-900	100
5	1500-1635	135
6	2280-2400	120
7($45°$)	800-900	100

Figure 1. An example of SCIAMACHY measurements: upper curve – cloudy scene, lower curve – clear sky case over the ocean (van Diedenhoven, 2007).

An example of SCIAMACHY hyperspectral measurements at the wavelengths $\lambda\lambda 800nm$ is shown in Fig.1. The general monotonous curve is due to multiple light scattering in the atmosphere and also in the underlying surface. The increase in the signal at wavelengths smaller than about 400nm is due to molecular scattering$\left(\because \lambda^{-4}\right)$ and rapid decrease below 330nm is due to the ozone absorption processes. Therefore, ozone and oxygen (still at smaller wavelengths) protect the biosphere from harmful UV-radiation. Gaseous absorption bands are clearly seen in the measured reflectance spectrum presented in Fig.1 along with several emission lines. The correspondent bands are used to estimate the trace gas abundances from satellite measurements using radiative transfer models.

3. Satellite retrievals of trace gas vertical columns

3. 1. O_3

SCIAMACHY continues the European global total ozone measurements that have been started with GOME in 1995 (Burrows et al., 1999). There are various methods for retrieving ozone total columns from GOME and SCIAMACHY (Bracher et al., 2005, Coldewey-Egbers et al., 2005, Weber et al., 2005, Eskes et al., 2005, van Roozendael et al. 2006, Balis et al., 2006, Lamsal et al., 2007). Our SCIAMACHY ozone retrieval algorithm is based upon the weighting function DOAS (WFDOAS) approach (Coldewey-Egbers et al., 2005, Weber et al., 2005, Bracher et al., 2005) that is similar to that described for greenhouse gases (see Section 3.4) but here applied in the UV spectral region (325-335 nm, see Fig.1), where Huggins ozone absorption bands are located. More than 90% of the column ozone resides in the stratosphere, so that some further steps are needed to extract the tropospheric O_3 amount from the vertical column. Total vertical columns of O_3, retrieved from SCIAMACHY measurements in October 2006 over Antarctic are presented in Fig.2. The ozone hole is clearly seen in the central part of the figure with ozone concentrations below 200DU (Dobson Units, 1 DU = 2.687×10^{16} molecules/cm^2).
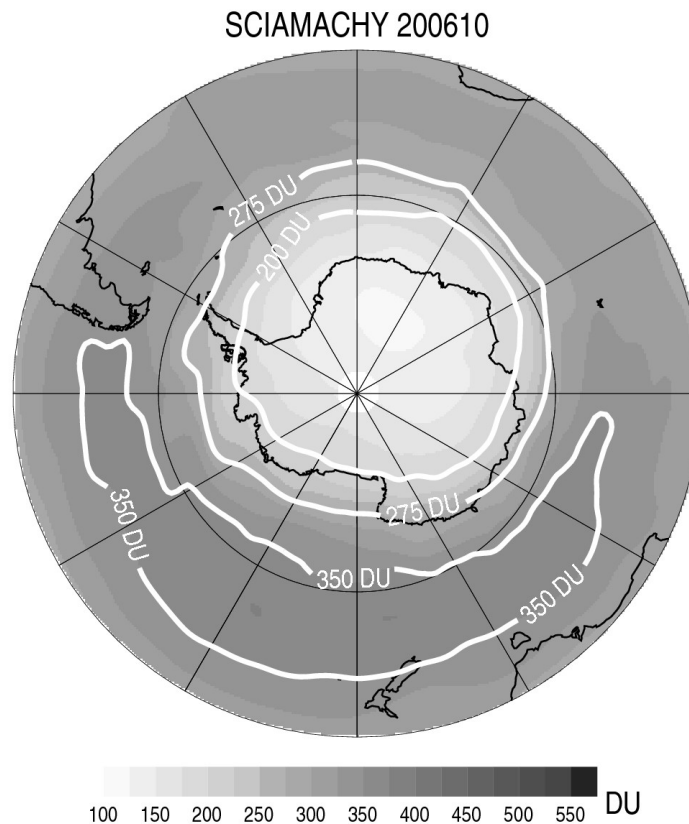

Figure 2. Total ozone distribution in October, 2006 over the southern pole as observed by SCIAMACHY.

Retrievals of ozone vertical columns are performed both for cloudless and cloudy conditions. In the case of clouds, their height and albedo are derived from oxygen A-band and the measurements in the visible, respectively. The ozone amount under the cloud is estimated using the concept of a ghost column (Coldewey-Egbers et al., 2005). The correspondent error in the ozone total VC due to assumptions on ghost vertical columns is low because most of ozone (>80%) is concentrated above clouds.

The tropospheric excess method is used to derive the tropospheric ozone concentration. This is an important task taking into account that ozone is a strong atmospheric pollutant. In the framework of this technique one subtracts from the total column an average total column from a reference region, where the tropospheric ozone is reduced to background values, e.g., in unpolluted areas. The reference region is preferably above the ocean, e.g., in Pacific (Burrows et al., 1999; Ladstätter et al., 2004, 2005). This method, however, assumes that the stratospheric column is nearly invariant between the reference region and the region of interest, which is a reasonable approximation only for tropical regions (Sierk et al., 2006; Ladstätter-Weißenmayer et al., 2007).

Biomass burning, often initiated in order to clear land for agricultural purposes, has been identified as a significant source of trace gases, which affect the atmosphere. Along with particulates, the major gases produced by biomass burning include carbon dioxide (CO_2), carbon monoxide (CO), methane (CH_4), formaldehyde (HCHO), oxides of nitrogen $NO_x(NO+NO_2)$ and ammonia (NH_3). The combination of CH_4, CO, nonmethane hydrocarbons (NMHC) and nitrogen oxides in the atmosphere leads to the photochemical production of tropospheric ozone. The lifetime of these ozone precursors and of ozone itself (Oltmans et al., 1998) is sufficiently long that they can be transported hundreds or even thousands of kilometers away from their source before being chemically destroyed or deposited. From GOME measurements increases of tropospheric amount of ozone were observed above Indonesia in September 1997, while only background amounts were measured in September 1998 (see Fig.3). As it follows from Fig.4, increases in the tropospheric ozone vertical columns can be seen over the central Africa in September 1997 as well. From GOME measurements an increase of tropospheric ozone amounts up to 50DU was observed (see Fig.4) caused mainly by biomass burning but also by biogenic emissions, lightning and stratospheric-tropospheric-exchange (Meyer-Arnek et al., 2005; Ladstätter-Weißenmayer et al., 2005). The current burden of tropospheric O_3 is about 370 Tg(O_3), which is equivalent to a globally averaged column density of 34 DU or a mean abundance of about 50 ppb (http://www.grida.no/climate/ipcc_tar/wg1/142.htm).

SCIAMACHY offers the unique possibility to combine limb and nadir ozone observations from the same instrument to retrieve the tropospheric ozone abundances. The alternating limb and nadir observation sequence of SCIAMACHY assures that after a limb observation sequence, the subsequent nadir sequence scans the same airmass (at the location of the tangent height of the prior limb scan). The simplest way to obtain the troposheric vertical column is to subtract the stratospheric column (from limb measurements) from the total column (from nadir measurements). Another and more involved approach is to use stratospheric and tropospheric air mass factors to determine the tropospheric column from the retrieved slant column as described by Sierk et al. (2006). First, a stratospheric slant column is determined using a stratospheric airmass factor from radiative transfer calculations with the stratospheric limb profile (von

Savigny et al., 2005) as input. This stratospheric slant column is then subtracted from the retrieved slant column (the standard DOAS fit in the nadir mode) to obtain the tropospheric slant column. Calculating now a tropospheric airmass factor (with some assumptions on the vertical distribution of ozone in the troposphere), the tropospheric slant column is converted into the tropospheric vertical column (Sierk et al., 2006). Principally this method is not limited to the tropical region. However, due to larger errors associated with the stratospheric limb ozone retrieval just above the tropopause, where the vertical ozone gradient is large, the errors in the tropospheric column can be large as well. Further research is underway to refine the technique for the tropospheric ozone retrievals from a satellite.

Summing up, Figs. 3, 4 show a large potential of satellite measurements for the tropospheric ozone monitoring from space.
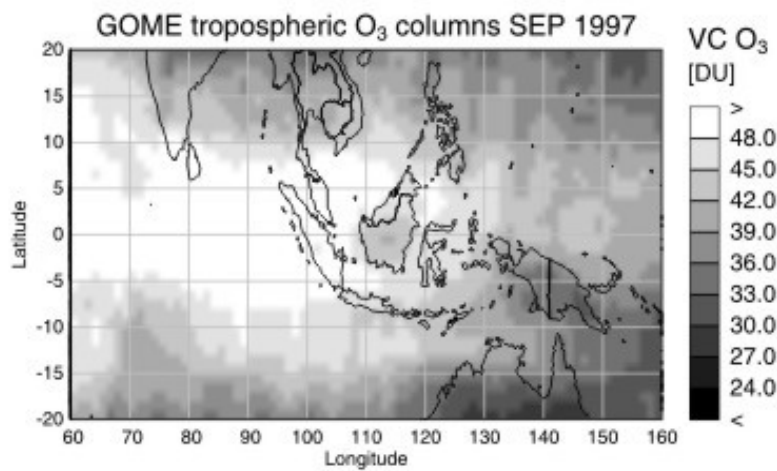

Figure 3a. Monthly mean tropospheric vertical columns of ozone (in DU), as retrieved from GOME measurements performed in September 1997 over Indonesia. Bright areas show enhanced tropospheric ozone abundances.
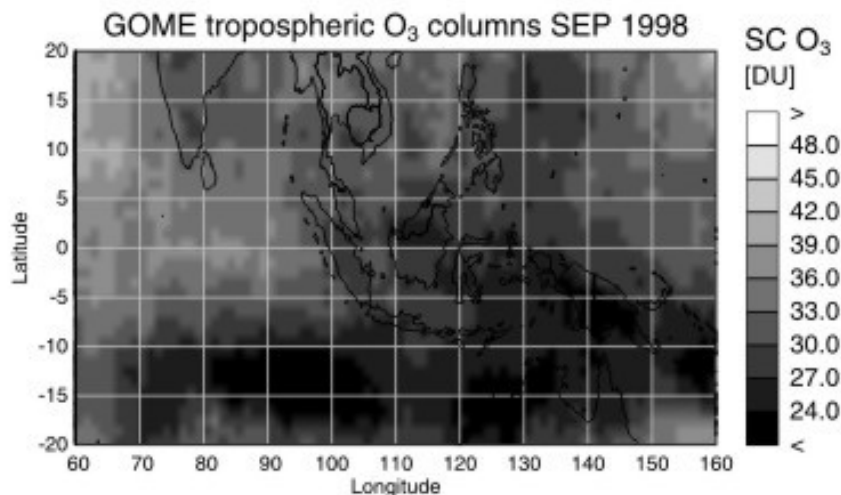

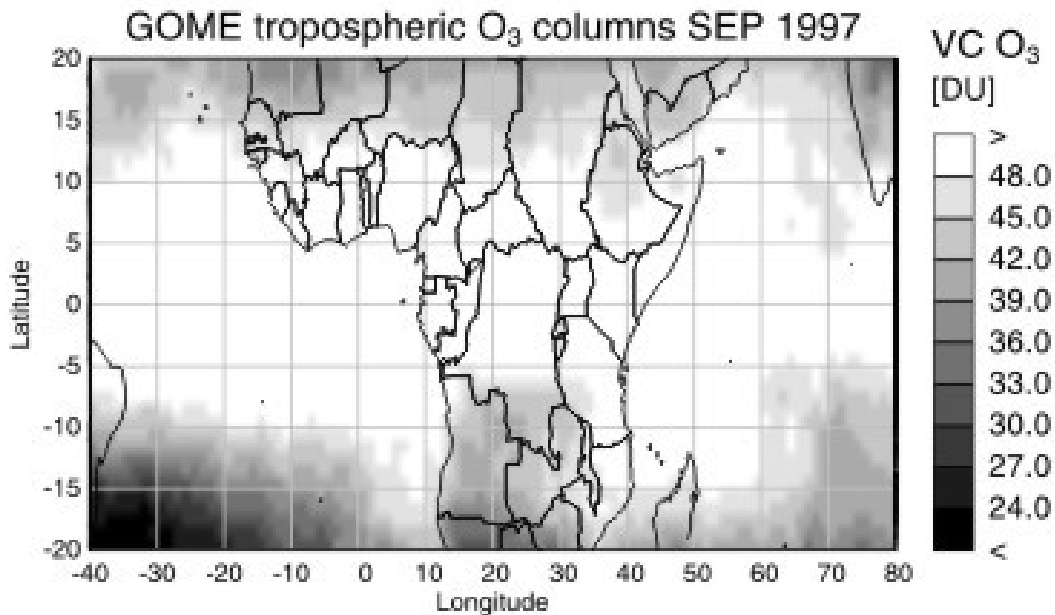**Figure 3b**. The same as in Fig. 3a except in 1998.

Figure 4. The monthly composite of the total column of tropospheric ozone (in DU) over Africa, for September 1997 as retrieved from GOME measurements.

3.2 NO_2

Nitrogen oxides are important trace gases in the troposphere. NO_x, being a key precursor of tropospheric ozone, leads to acid rain formation and eutrophication and directly and indirectly contributes to radiative forcing. The sources of NO_x are both natural and anthropogenic, the latter dominating in industrialized regions. Most of the NO_x is emitted from combustion processes (fossil fuel use, biomass burning) in the form of NO, but microbial soil emissions and lightning sources also contribute.

Nitrogen dioxide (NO_2) has strong absorption bands in the blue spectral range (see Table 1), which makes it accessible to DOAS measurements (Platt, 1994). As photons reach the surface at these wavelengths, both, the stratospheric and the tropospheric NO_2 can be retrieved from satellite measurements of scattered sunlight. This has been first demonstrated on data from the Global Ozone Monitoring Experiment (Leue et al., 2001; Richter et al., 2002), which provided the first global maps of tropospheric NO_2 burden. The SCIAMACHY instrument is very similar to GOME but offers much better spatial resolution (30 x 60 km^2 as compared to 40 x 320 km^2 for GOME) facilitating identification of source regions down to city scales.

An example of a SCIAMACHY global tropospheric NO_2 map is shown in Fig.5. Industrialized regions can clearly be identified as regions with strongly enhanced NO_2 vertical columns in the US, Europe and parts of Asia. In addition, areas with intense biomass burning in South America, Africa and the Pacific region also have larger NO_2 vertical columns. Closer inspection also shows the effect of emissions from international shipping, in particular, from the south tip of India towards Indonesia, where heavy vessel traffic in a very limited corridor leads to large local enhancements of NO_2 levels in the otherwise pristine marine boundary layer (Richter et al., 2004; Beirle et al., 2004).

The combined data set of GOME and SCIAMACHY is now extending over more than one decade. This data series can be used to investigate temporal changes in NO_2. As the lifetime of NO_2 is rather short in the boundary layer (of the order of hours), the NO_2 columns are in good approximation linearly related to emissions of NO_x (Martin et al., 2003). Therefore, changes in NO_2 columns observed from space can be interpreted in terms of changes in emissions, and this has been applied to different regions. One example is the study of emission changes in Asia. Since 1995, the year of GOME launch, parts of China have been rapidly industrializing. The corresponding increase in fossil fuel use lead to large increases in NO_x emissions as well as in emissions of other trace gases and particulate matter potentially hazardous for local population. This is evident from direct comparison of satellite NO_2 maps which had only moderate NO_2 vertical columns over China in 1996 but by far larger columns in 2006. The year-by-year change of the NO_2 columns above China relative to 1996 is shown in Fig.6, which is an extension of the work published in Richter et al. (2005). Clearly, NO_2 columns have been increasing exponentially but appear to level off in 2006. This result still has to be confirmed but could be related to the increased efforts for emission reductions by the Chinese government and gradual switch to cleaner fuels. In a recent study (Zhang et al., 2007), the satellite based emission changes have been compared to a detailed bottom-up inventory of NO_x emissions in China, and good agreement was found. In particular for the summer values, the two approaches lead to agreement within the error bars, while in winter the satellite data argue for a larger increase. This could be related to larger retrieval uncertainties in winter but could also reflect real changes in emissions in winter, e.g., due to heating, which are not yet included in the emission inventories.
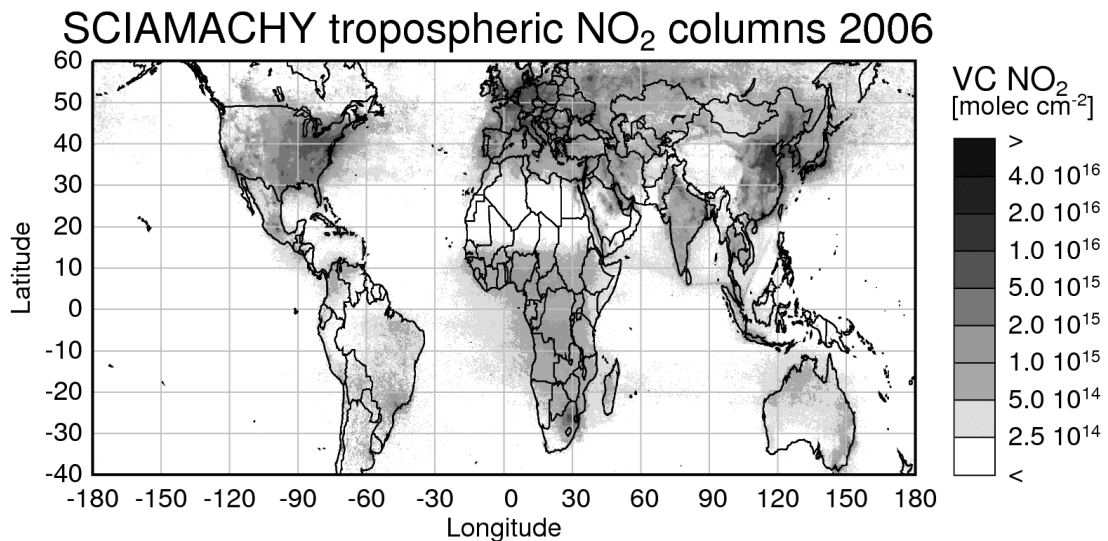

Figure 5. Annual average of tropospheric NO_2 columns for 2006 derived from measurements of the SCIAMACHY instrument. Please note the logarithmic scale. Large columns are mainly observed over industrialized areas in North America, Europe, and Asia.
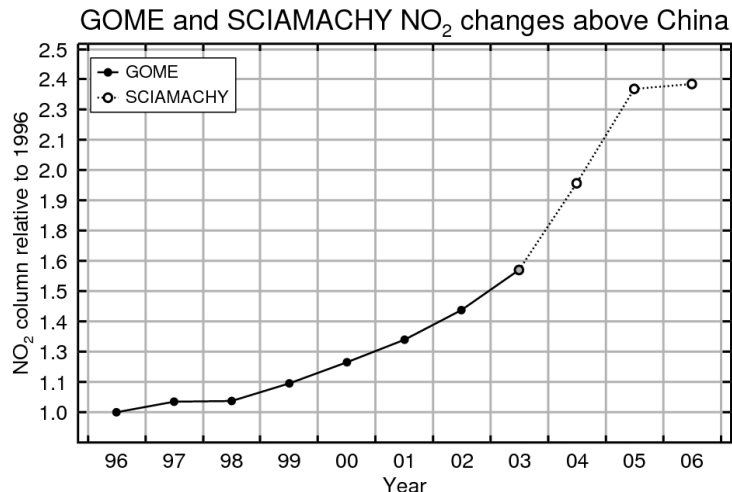
GOME and SCIAMACHY NO$_2$ changes above China

Figure 6. Change of annual NO$_2$ columns over East Central China (30°N to 40°N, 110°E to 123°E) relative to measurements in 1996. Data before 2003 are from GOME, data for the more recent years are from SCIAMACHY. The slow down in emission increases in 2006 still has to be confirmed.

3.3 SO$_2$

Sulfur dioxide (SO$_2$) is emitted into the atmosphere by volcanic eruptions and degassing and also by burning of fossil fuels, in particular coal and smeltering of sulfur rich ores. In the troposphere, SO$_2$ is relevant as it leads to the formation of H$_2$SO$_4$ which is responsible for acid rain formation and plays a key role in the formation of anthropogenic aerosols. Both through aerosol formation and by acting as cloud condensation nuclei, it is involved in radiative forcing. In addition, SO$_2$ adversely affects human health, in particular, during smog events.

Atmospheric sulfur dioxide amounts can be determined by absorption spectroscopy in the UV spectral range (see Table 1), where the molecule has strong differential absorption features. From space, this was first demonstrated using Total Ozone Mapping Spectrometer (TOMS) data (Krueger et al., 1995), which have good spatial resolution but limited sensitivity as result of the poor spectral resolution. Using GOME data, it was for the first time possible to identify the emissions of large coal fired power plants (Eisinger et al., 1998) and SCIAMACHY provides similar sensitivity but at much improved spatial resolution (Afe et al., 2004). However, compared to the retrieval of NO$_2$, the sensitivity to the lowest atmospheric layers is reduced as Rayleigh scattering is much more efficient at the wavelengths (see Table 1 and also Fig.1) used in the data analysis. Also, the amount of available light is reduced for a number of reasons. Therefore, small amounts of SO$_2$ can not be accurately determined from a satellite at present.

In Fig.7, a global map of SO$_2$ vertical columns is shown for the year 2006. This figure is still not fully quantitative as a constant airmass factor has been used in spite of large differences in sensitivity for high altitude emissions (e.g., volcanic eruptions) and surface signals (e.g., local pollution). However, the overall pattern with signatures from several volcanic sources, pollution from coal burning (mainly in China and to a smaller degree also in the US and Eastern Europe) and the emissions of smeltering can clearly be identified.

As has already been discussed in the section on NO_2, fossil fuel use in China has much increased over the last decade. As a large fraction of this is based on sulfur rich coal, a significant increase in SO_2 signal is also observed. This is shown in Fig.8 for a combined GOME and SCIAMACHY time series, and an evolution can be observed, which is quite similar to that of NO_2, including the slow down in increase in 2006. However, in contrast to NO_2, this curve can not simply be interpreted as an emission increase as the sensitivity of the satellite measurements of SO_2 over China close to the surface is low. Therefore, recent changes in the coal use from domestic heating (emission close to the surface) to power plants (emission from high stacks) could potentially impact on the results of satellite retrievals. This aspect is currently being investigated in more detail.
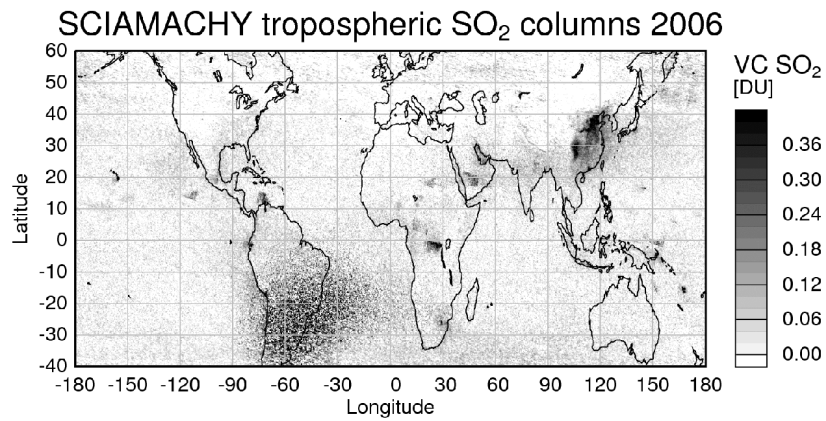

Figure 7. Annual average of tropospheric SO_2 columns for 2006 derived from measurements of the SCIAMACHY instrument. The large scatter over Southern America is the result of an anomaly in the Earth's magnetic field and not related to SO_2 in the atmosphere.
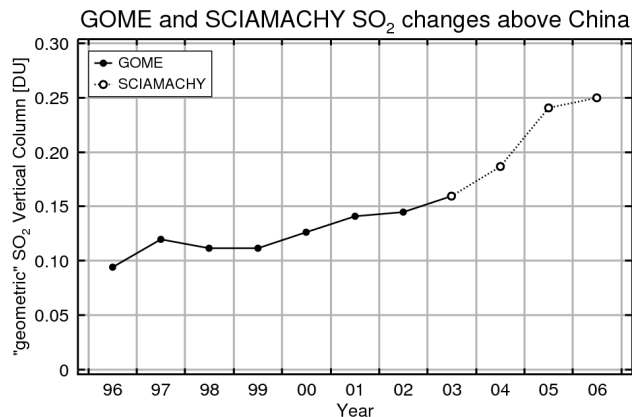

Figure 8. Change of annual SO_2 columns over East Central China (30°N to 40°N, 110°E to 123°E). Data before 2003 are from GOME, data for the more recent years are from SCIAMACHY. The absolute values still need to be corrected for lower sensitivity of the measurements close to the surface The slow down in emission increases in 2006 still has to be confirmed.

3.4 Carbon gases: CO_2, CH_4, and CO

The three carbon (atom containing) gases, namely, carbon dioxide, methane and carbon monoxide are important atmospheric constituents affecting climate and air quality. The near-infrared nadir spectra measured by SCIAMACHY on ENVISAT contain information on the vertical columns of these gases (see Table 1). To retrieve this information the Weighting Function Modified Differential Optical Absorption Spectroscopy (WFM-DOAS or WFMD) retrieval algorithm (Buchwitz et al., 2006, 2007a, 2007b) has been developed at the University of Bremen. Main data products are carbon monoxide vertical columns (in molecules/cm^2) and dry-air column averaged mixing ratios of the greenhouse gases CO_2 and CH_4, denoted XCO_2 (in ppm) and XCH_4 (in ppb), respectively. The mixing ratio is defined as the ratio of the VC of the correspondent trace gas (in molecules/cm^2) to the total VC of the atmospheric air $\left(c\ 2.148\ 10^{25}\,\text{moleclules/cm}^2 \text{ for the atmospheric column above sea level} \right)$. The main goal of satellite retrievals is to achieve a data quality high enough such that quantitative information of the surface sources and sinks of trace gases such as CO, CO_2, and CH_4 can be obtained, for example, via inverse modeling.

Different groups have developed somewhat different retrieval approaches to retrieve carbon monoxide (Buchwitz et al., 2000, 2006, and 2007a; Frankenberg et al., 2005a; Gloudemans et al., 2006; de Laat et al., 2006), methane (Buchwitz et al., 2000 and 2006; Frankenberg et al., 2005b and 2006), and carbon dioxide (Buchwitz et al., 2000 and 2007b; Barkley et al., 2007) columns or column-averaged mixing ratios from the SCIAMACHY spectral data. Here we limit the discussion to the data products generated at the University of Bremen.

Recently three years of SCIAMACHY data (2003-2005) have been reprocessed with the latest version of the University of Bremen WFM-DOAS retrieval algorithm, namely version 0.6 for CO and version 1.0 for the greenhouse gases CO_2 and CH_4.

Details about the new WFM-DOAS version 0.6 carbon monoxide data set are given by Buchwitz et al.(2007a). There it is shown that the accuracy of the CO column data set is about 10-20% as concluded from a comparison with independent satellite data (MOPITT) and ground based FTS measurements. Figure 9a shows the global distribution of the CO column as retrieved from SCIAMACHY for the year 2004. As can be seen, the inter-hemispheric gradient as well as major CO source regions such as China and central Africa can be clearly identified. When averaging long time series, it is also possible to detect elevated CO vertical columns over highly populated areas such as individual cities (Buchwitz et al., 2007a).

Figure 9b shows the global distribution of the column-averaged mixing ratio of methane for the year 2004. The SCIAMACHY methane retrievals have been strictly quality filtered in order to meet quite demanding precision and accuracy requirements on the order of 1%. This results in data gaps (shown in white) even in the yearly average. As can be seen, the inter-hemispheric gradient as well as major source regions such as China (e.g., rice emissions), Siberia (wetland emissions), and the tropical rain forest region (e.g., wetland and possibly plant emissions) are clearly visible. Detailed results concerning the new methane data set have not yet been published but a first comparison with ground based FTS measurements (Dils et al., 2006) and ongoing analysis clearly shows a significantly improved accuracy compared to the earlier algorithm version WFMD 0.5 described in Buchwitz et al. (2006), mainly due to the use of better calibrated

SCIAMACHY top-of-atmosphere nadir reflectance spectra (Kokhanovsky et al., 2007c). Current investigations focus on assessing the accuracy and precision of regionally resolved XCH_4, for example, by comparison with global model data such as TM5 (see Buchwitz et al., 2006). Comparisons show that all major methane source regions can be clearly detected. In line with previous studies we see significantly elevated methane over the tropics compared to current models using current emissions data bases, confirming earlier studies. The data quality is high enough such that first inverse modeling attempts to quantify methane emissions are undertaken using this new data set. The first ever inverse modeling of methane surface fluxes using satellite data has been performed by Bergamaschi et al. (2007), using the methane satellite data described in Frankenberg et al. (2006).

First results concerning the new global CO_2 data set are shown in Buchwitz et al. (2007b), focusing on northern hemispheric large scale features such as the CO_2 seasonal cycle (mainly caused by CO_2 uptake and release by the growing and decaying vegetation) and the year-to-year CO_2 increase (mainly caused by the burning of fossil fuels), which can be detected with SCIAMACHY as also shown in Fig.9c. Current investigations focus on assessing the accuracy and precision of regionally resolved XCO_2, for example, by comparison with global model data.
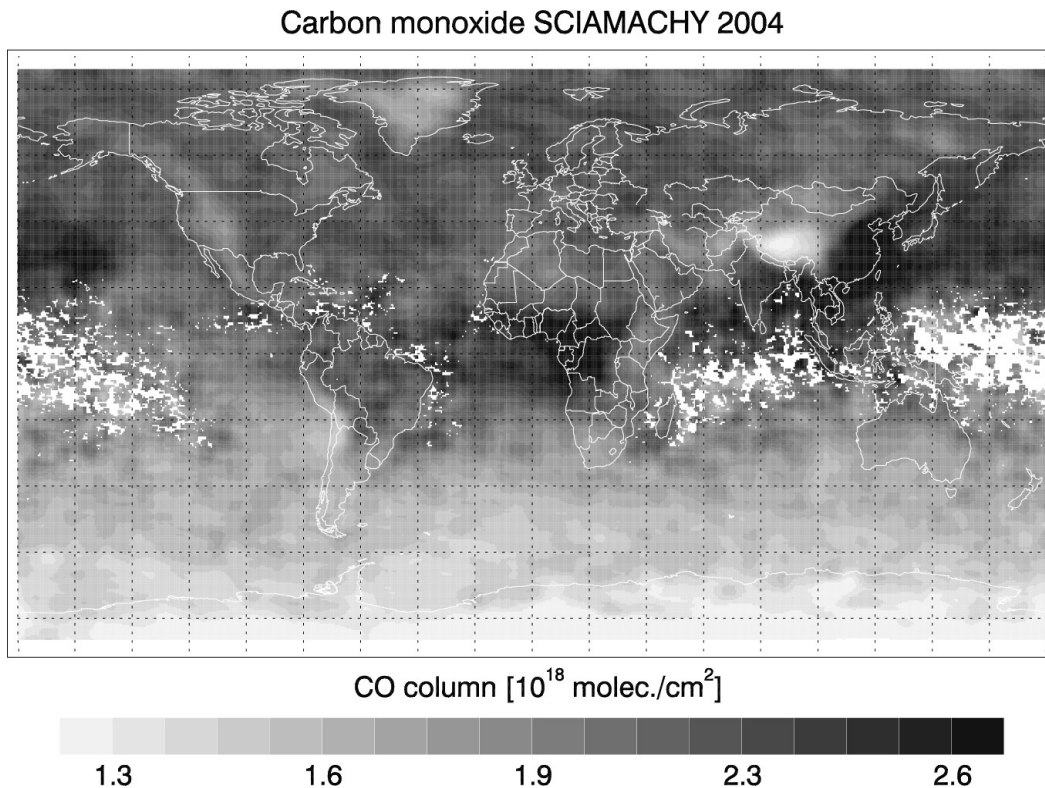

Figure 9a. Carbon monoxide vertical columns as retrieved from SCIAMACHY for the year 2004. Clearly visible is the inter-hemispheric gradient, with higher CO over the northern hemisphere, and major CO source regions such as China and central Africa.
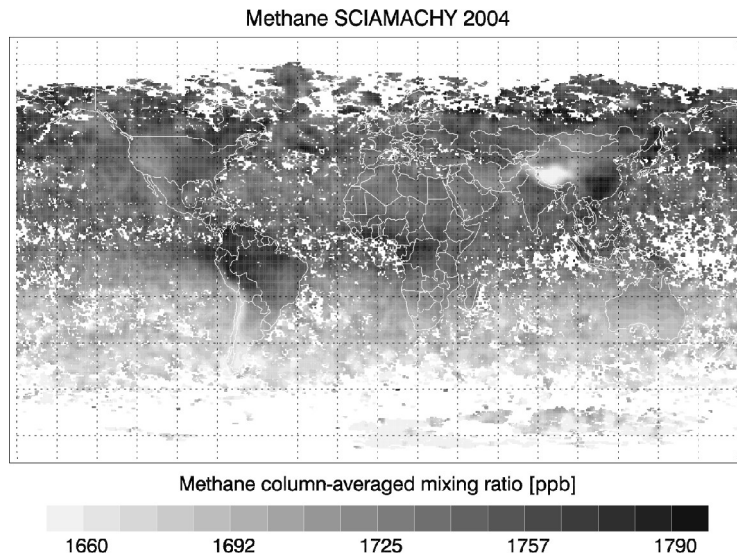
Methane SCIAMACHY 2004

Methane column-averaged mixing ratio [ppb]

| 1660 | 1692 | 1725 | 1757 | 1790 |

Figure 9b. Column-averaged mixing ratios of methane as retrieved from SCIAMACHY for the year 2004. Clearly visible is the inter-hemispheric gradient, with higher methane over the northern hemisphere, and major methane source regions such as China, parts of Siberia and parts of the tropics.
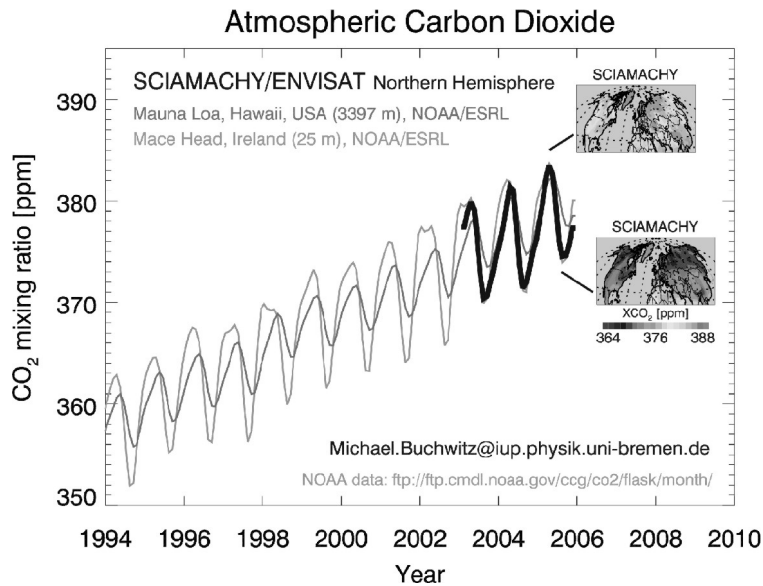

Atmospheric Carbon Dioxide

Figure 9c. Mixing ratios of northern hemispheric carbon dioxide. The two maps (top right) show the spatial distribution of the column averaged mixing ratios of CO_2, denoted XCO_2, as retrieved from SCIAMACHY, for months March-June (top map) and July-October (bottom map) of 2005. The thick black line shows the time dependence of the northern hemispheric monthly mean values derived from SCIAMACHY measurements. Satellite data confirm the carbon dioxide seasonal cycle and the CO_2 year-to-year increase first observed using ground-based measurements. For comparison, NOAA/ESRL/GMD CO_2 surface measurements at two stations based on weekly flask

sampling are also shown (thin lines; courtesy T. J. Conway, NOAA/ESRL/GMD). More details are given by Buchwitz et al (2007b).

3.5 H_2O

Water vapor is an important greenhouse gas, which also plays a major role in atmospheric chemistry and thermodynamics. Satellite observations of H_2O have quite a long history with different wavelength ranges used for humidity monitoring including microwaves, IR and the visible.

SCIAMACHY water vapor is retrieved using a derivation of the standard Differential Optical Absorption Spectroscopy method, which is called Air Mass Corrected (AMC-) DOAS. The AMC-DOAS method has been originally applied to GOME measurements in the visible spectral region (688-700 nm) (see e.g. Noël et al., 1999). Subsequently, the algorithm was adapted to work on SCIAMACHY and, most recently, also on GOME-2 data (see, e.g., Noël et al., 2004, 2005, 2007).

With the AMC-DOAS algorithm it is possible to derive total water vapor columns over all surfaces (land or ocean) during daytime. The limitation is due to the possible presence of clouds. The algorithm is intended to work only for cloudless atmosphere. Therefore, the results could potentially have dry bias. Also measurements with SCIAMACHY are performed almost at the same local time at a given location (10:00 local equator crossing time). Therefore, the diurnal variation is not captured. The same problem exists with other SCIAMACHY trace gas vertical columns. The future geostationary chemistry missions can resolve this problem.

In contrast to, e.g., most water vapor data sets based on measurements in the microwave spectral region, the AMC-DOAS method does not rely on external calibration sources like radio sonde data. The GOME and SCIAMACHY water vapor columns, therefore, provide a completely new and independent data source. The AMC-DOAS method is very insensitive to instrumental features and calibration issues. This facilitates the combination of the AMC-DOAS results of different instruments (like GOME and SCIAMACHY). Fig.10 shows a comparison between global GOME and SCIAMACHY water vapor data from August 2002 until end of 2003. The black dots denote the (globally averaged) mean deviation between GOME and SCIAMACHY, the vertical bars are the corresponding standard deviations. The thick gray line shows the monthly mean deviations. Note that SCIAMACHY data of 2002 are of slightly reduced quality because of the non-availability of an actual solar spectrum. Furthermore, GOME data after June 2003 have no longer global coverage due to the problem with the ERS-2 tape recorder. As can be seen from Fig.10, the GOME and SCIAMACHY data agree on average quite well, but there is a considerable scatter of about 0.2-0.3 g/cm^2 in the data. This scatter is mainly related to the large temporal and spatial variability of water vapor, which generally makes comparisons between water vapor measurements of different sensors very difficult.

By the combination of the AMC-DOAS water vapor results for the different instruments a global water vapor climatology can be derived, starting with GOME measurements in 1995 and continuing with SCIAMACHY since 2002. Figure 11 shows as an example the derived annual mean water vapor concentrations for the years 1996 to 2006. The white areas over high mountain regions (like the Himalaya) denote missing data. These data have been sorted out by the inherent AMC-DOAS quality check (see, e.g., Noël et al., 2004), which also eliminates cloudy scenes.

The annual mean water vapor maps show the typical global distribution patterns of water vapor, which remain quite stable throughout the years. There are high concentrations of up to about 6 g/cm^2 in the tropical regions; this enhanced water vapor band coincides with the Inner Tropical Convergence Zone and, thus, moves with season in North/South direction. Towards higher latitudes the water vapor columns are much smaller, reaching values well below 1 g/cm^2. There is also a seasonal variation in these regions, but this, of course, can not be seen from the annual means. As expected, there is a correlation of water vapor maps with the correspondent global maps of cloudiness derived from SCIAMACHY measurements (Kokhanovsky et al., 2007d).

The water vapor time series will be extended by further SCIAMACHY measurements and by measurements of GOME-2 on the series of meteorological satellites MetOp of which the first one was successfully launched in October 2006. With GOME-2/MetOp, a continuation of the AMC-DOAS water vapor data set until at least 2020 can be expected.

The resulting AMC-DOAS water vapor climatology will be useful for climatologic studies of the water cycle. This has been already shown by a first application, namely the derivation of global and local water vapor trends over the time interval from 1996 to 2006 (Mieruch et al., 2007). In this study several regions on the Earth have been identified, which show significant changes of the water vapor VC, reaching several percents per year when assuming a linear trend over 11 years. These results need, however, to be confirmed by further studies based on extended data sets, i.e., longer time series.
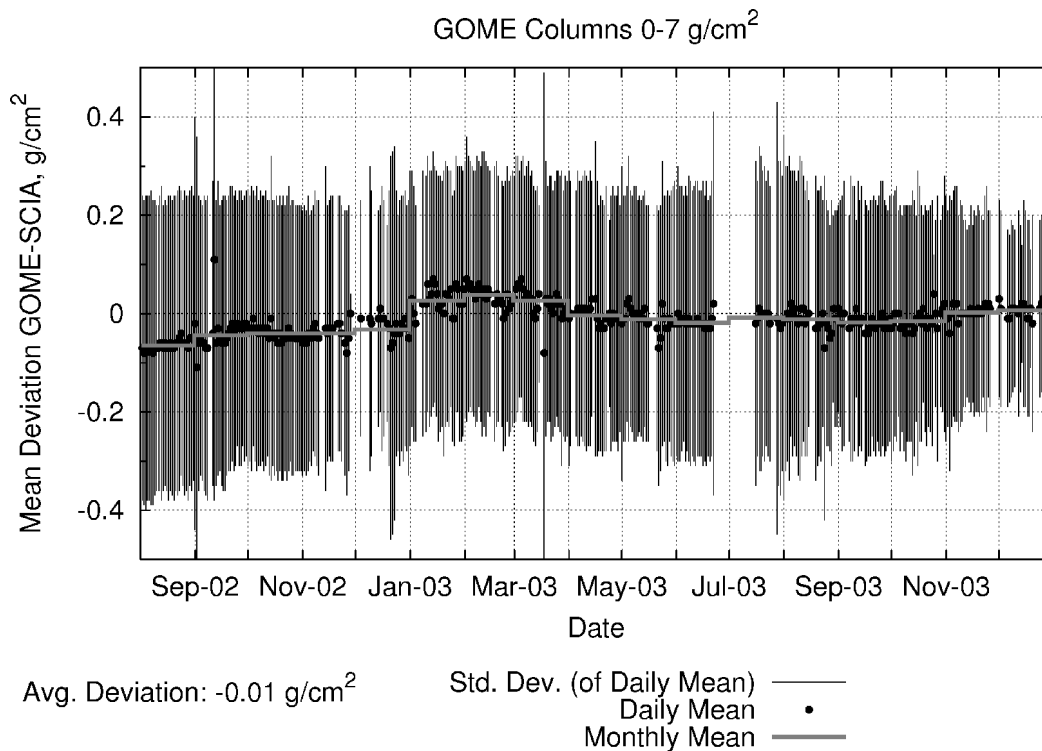

Figure 10. Comparison between GOME and SCIAMACHY water vapor data.
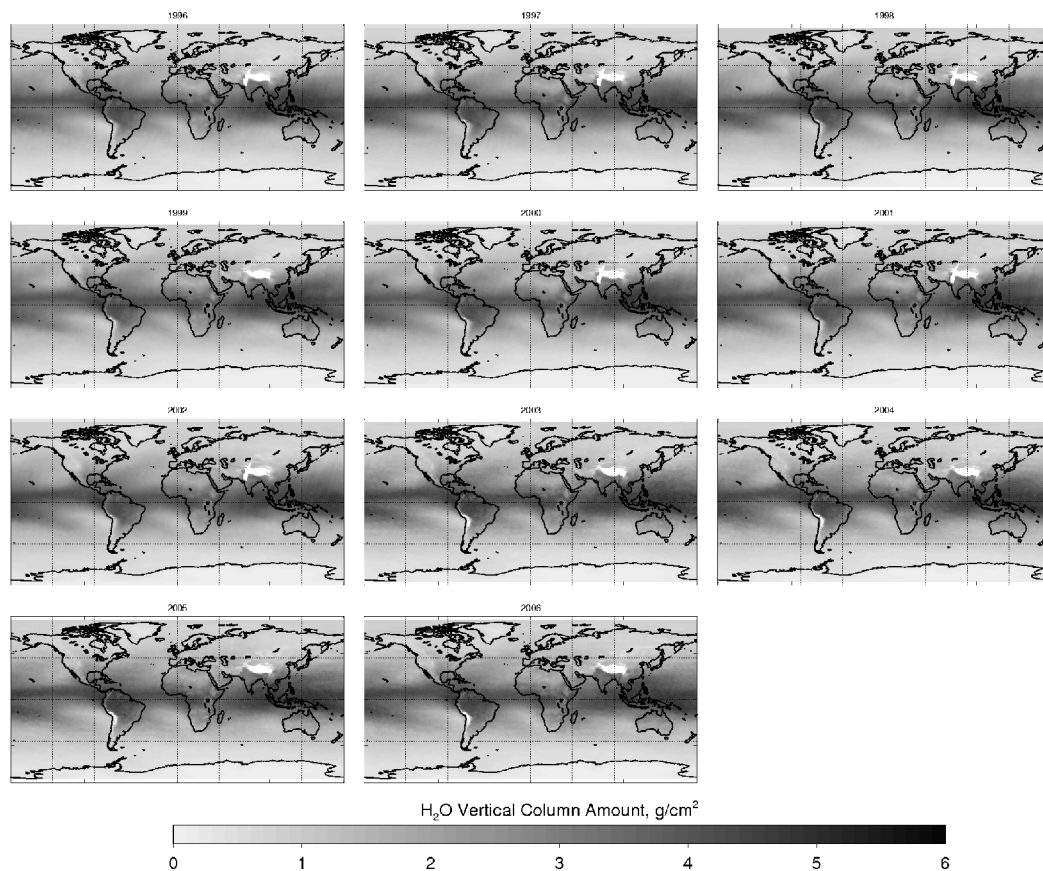
Figure 11. Global maps of annual mean water vapor total columns derived from the combined GOME (1996-2002) and SCIAMACHY (2003-2006) measurements using the AMC-DOAS method.

4. Aerosols

Atmospheric gases do not exist in the atmosphere in a stationary state. Their concentration changes due to the presence of various sources and sinks. An important factor is the interaction of gases with cloud droplets and ice crystals and also with aerosols. For instance, gases can easily be dissolved in water droplets, therefore, forming new chemical substances. Subsequently, the evaporation of water from droplets leads to the formation of aerosol particles from correspondent newly born substances. Therefore, the global distribution of cloudiness (Kokhanovsky et al., 2007d) is relevant not only for climate and weather issues but also for atmospheric chemistry (e.g., lightning effects and NO_2 production, etc.). Also aerosols and clouds in the satellite ground scene must be monitored to increase the accuracy of trace gas VC retrieval algorithms (Kokhanovsky et al., 2007a). This is done either using the data from the same spectrometer as used for monitoring of trace gases or through the synergetic use of other instruments installed on the same space platform. Information from instruments (e.g., with high spatial resolution, 0.1-1.0km^2) onboard other satellites can be used for this purpose as well.

Yet another important topic of current atmospheric research is the study of heterogeneous chemical reactions of gases with atmospheric particulate matter. For instance, soot participates in chemical reactions with gases discussed above (e.g., NO_2, SO_2, O_3). The total surface area of particles is of great importance for the estimation of the rate and effectivity of correspondent chemical reactions. There are several attempts to retrieve the average size and surface area s of particles suspended in atmosphere from satellite measurements. In particular, Kokhanovsky et al. (2006) introduced the technique based on multi-spectral SeaWiFs observations with the spatial resolution of 1km^2. SCIAMACHY resolution is too coarse to derive aerosol properties because most pixels are contaminated by clouds making aerosol retrievals possible only on rare occasions.

The technique is based on the fact that the average radius of particles (and, therefore, s) can be easily determined from the spectral slope of the aerosol optical thickness τ, which is the standard product of many satellite retrieval algorithms. In particular, calculations according to Mie theory (van de Hulst, 1957) suggest that the following relationship between the effective radius a_{ef} of particles ($a_{ef} = 3v/s$, where v is the average volume of scatterers) and the Ångstrom spectral exponent α holds in good approximation:

$$a_{ef} = 0.62\exp(-1.18\alpha) + 0.21\exp(-5.84\alpha),$$ (3)

where

$$\alpha = A \ln \frac{\tau(\lambda)}{\tau(\lambda_0)} ,$$ (4)

$A = \ln^{-1}(\lambda_0/\lambda)$, $\lambda_0 = 412nm$, $\lambda = 670nm$, and a_{ef} is expressed in μm. It was assumed in the derivation of Eq. (3) that the size distribution of aerosol particles is given by the lognormal law with the coefficient of variance equal to the average radius of aerosol particles and the refractive index of aerosol particles equal to 1.45+0.005i (see, Kokhanovsky et al. (2006) for details). The comparison of exact and approximate calculations using Eq. (3) is given in Fig.12. Knowing the effective radius, one can also estimate the average extinction cross section σ of aerosol particles and, therefore, the particle columnar number concentration: $n = \tau/\sigma$ (for a homogeneous aerosol layer). Clearly, this enables also the calculation of columnar particulate matter mass PM10 (assuming the aerosol density and using retrieved a_{ef}) and also the columnar aerosol surface. Humidity corrections and boundary layer height measurements are needed to bring results in correspondence with ground techniques usually performed for the case of dry aerosol at the height of 2m above the surface.

The example of retrieved spatial distribution of the aerosol optical thickness at the wavelength 412nm, where the surface contribution to the satellite signal is low, using the Medium Resolution Imaging Spectrometer (MERIS) onboard ENVISAT data over Eastern Europe is shown in Fig.13, where the extended pollution plume is clearly seen in the middle of the picture. Fig.14 gives the retrieval of aerosol optical thickness over Mexico. Selected areas in Fig.14 give positions of highly polluted cities (Guadalajara, Leon and Mexico City, left to right on the figure). The PM10 retrieved over Mexico City is given in Fig. 15. The spectral aerosol optical thickness used for PM10 retrievals was determined applying the Bremen Aerosol Retrieval Algorithm (von Hoyningen-Huene et

al., 2003). The algorithm is based on the analysis of the absolute top-of-atmosphere reflectance measurements.

Clearly, larger aerosol amounts over black ground (as usually the case over land at 412nm) correspond also to larger values of top-of-atmosphere reflectance. Therefore, τ (and also α) can be retrieved using information on the spectral reflectance as measured by a satellite instrument. The results presented confirm a high potential for monitoring of aerosol optical thickness and particulate matter concentration from space. However, further validation of results using, in particular, ground based measurements is needed (Remer et al.,2005; Kokhanovsky et al., 2007e, von Hoyningen-Huene et al.,2007).
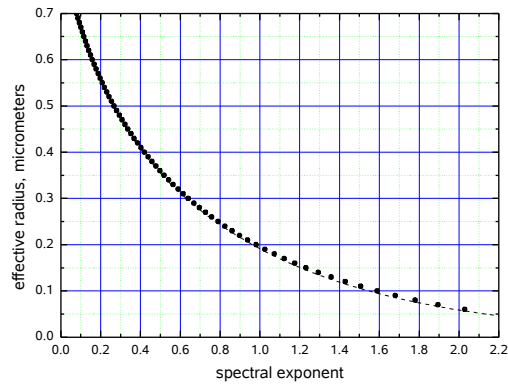

Figure 12. Dependence of the spectral exponent on the effective radius of aerosol particles calculated using Mie theory (symbols). The dashed line corresponds to Eq. (3).
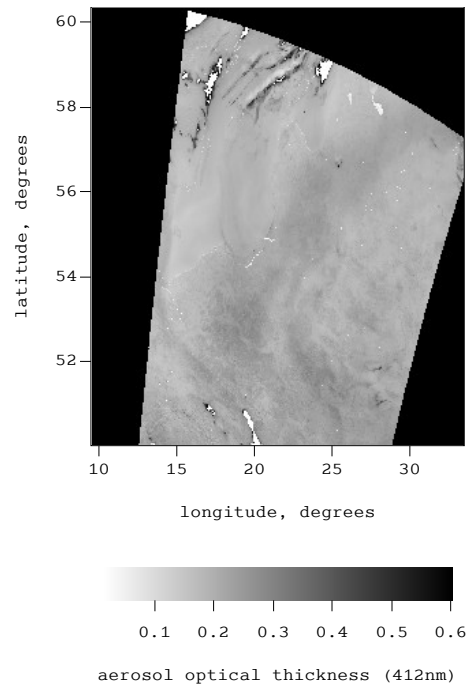

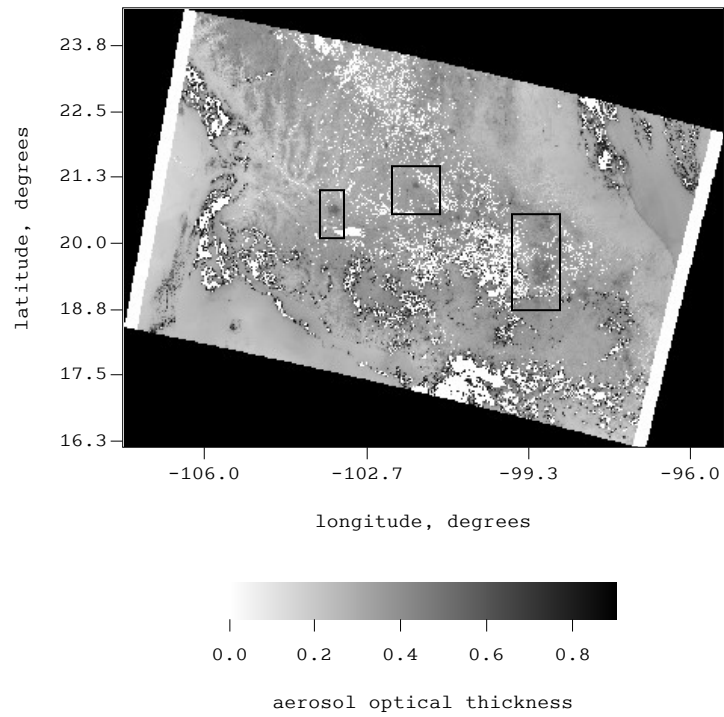**Figure 13**. Aerosol optical thickness at 412 nm over Eastern Europe on October 11, 2005.

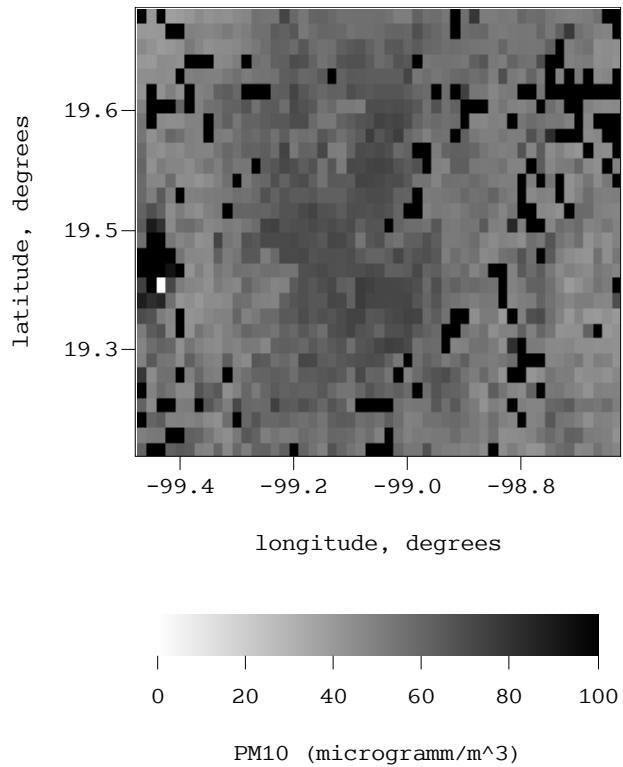**Figure 14.** Aerosol optical thickness at 412nm over Mexico on January 12, 2005.

Figure 15. PM10 retrieved over Mexico City using MERIS data.

5. Conclusions

A major conclusion of this work is that current level of understanding of light scattering and absorption in atmosphere, ocean, and land surface coupled with modern computer and satellite technology is such that accurate satellite retrievals of vertical total and tropospheric columns of trace gases and aerosols are possible. In some cases, the vertical profiling of trace gas concentrations can be performed. The results of retrievals can be used for the analysis of pollution transport, climate change problems and monitoring particular atmospheric events. The satellite retrieval results are accessible to the scientists and general public via several websites, e.g.,

- http://www.iup.uni-bremen.de/
- http://daac.gsfc.nasa.gov/techlab/giovanni/
- http:/www.temis.nl/

The accuracy of the retrievals is highly dependent on the trace gas under study. The relative errors are below 1-3% for XCH_4 and XCO_2. They are smaller than 3-5% for O_3 depending on the solar zenith angle. For the water vapor, relative errors are smaller than 5% for vertical columns larger than $0.6 \, g/cm^2$. They increase up to 10% for smaller values of water vapor vertical columns. Such a high accuracy of retrievals for NO_2 and SO_2 vertical columns is not possible with the start-of-art satellite retrieval algorithms. In particular, relative errors for the retrieved NO_2 vertical columns can reach 60% . They are even larger (up to 100%) for SO_2. Nevertheless, even in this case satellite retrievals give important information on temporal trends and the spatial distribution of pollution, which can not be derived by other means at present.

A major concern is that measurements are performed at a small repetition rate and also with rather large spatial resolution. The problem will be overcome in future satellite missions operating from geostationary orbits. Correspondent data will enable much better understanding of atmospheric composition, relevant processes and climate change issues.

7. References

Afe, O. T., A. Richter, B. Sierk, F. Wittrock, and J. P. Burrows, 2004, BrO emission from volcanoes - a survey using GOME and SCIAMACHY measurements, *Geophys. Res. Lett.* **31**, L24113, doi:10.1029/2004GL020994.

Balis, D., J.-C. Lambert, M. Van Roozendael, R. Spurr, D. Loyola, Y. Livschitz, P. Valks, V. Amiridis, P. Gerard, J. Granville, and C. Zehner, 2007, Ten years of GOME/ERS2 total ozone data: The new GOME data processor (GDP) version 4: 2. Ground-based validation and comparisons with TOMS V7/V8, *J. Geophys. Res*., **112**, doi:10.1029/2005JD006376.

Barkley, M. P., P. S. Monks, A. J. Hewitt, T. Machida, A. Desai, N. Vinnichenko, T. Nakazawa, Yu. M. Arshinov, N. Fedoseev, and T. Watai, T., 2007, Assessing the near surface sensitivity of SCIAMACHY atmospheric CO_2 retrieved using (FSI) WFM-DOAS, *Atmos. Chem. Phys. Discuss*. **7**: 2477-2530.

Beirle, S., U. Platt, R. von Glasow, M. Wenig, and T. Wagner, 2004, Estimate of nitrogen oxide emissions from shipping by satellite remote sensing, *Geophys. Res. Lett.*, **31**, L18102, doi:10.1029/2004GL020312.

Bergamaschi, P., C. Frankenberg, J. F. Meirink, M. Krol, F. Dentener, T. Wagner, U. Platt, J. O. Kaplan, S. Körner, M. Heimann, E. J. Dlugokencky, A. and Goede, 2007, Satellite chartography of atmospheric methane from SCIAMACHY onboard ENVISAT: 2. Evaluation based on inverse model simulations, *J. Geophys. Res*. **112**, D02304, doi:10.1029/2006JD007268.

Bracher, A., L.N. Lamsal, M. Weber, K. Bramstedt, M. Coldewey-Egbers, and J. P. Burrows, 2005, Global satellite validation of SCIAMACHY O_3 columns with GOME WFDOAS, *Atmos. Chem. Phys.* **5**: 2357-2368.

Buchwitz, M., V. V. Rozanov, and J. P. Burrows, 2000, A near – infrared optimized DOAS method for the first global retrieval of atmospheric CH_4, CO, CO_2, H_2O, and N_2O total column amounts from SCIMACHY Envisat-1 nadir radiances, *J. Geophys. Res*. **105**: 15231-15245.

Buchwitz, M., R. de Beek, S. Noël, J. P. Burrows, H. Bovensmann, O. Schneising, I. Khlystova, M. Bruns, H. Bremer, P. Bergamaschi , S. Körner, and M. Heimann, 2006, Atmospheric carbon gases retrieved from SCIAMACHY by WFM-DOAS: version 0.5 CO and CH_4 and impact of calibration improvements on CO_2 retrieval, *Atmos. Chem. Phys*. **6**: 2727-2751.

Buchwitz, M., I. Khlystova, H. Bovensmann, and J. P. Burrows, 2007a, Three years of global carbon monoxide from SCIAMACHY: Comparison with MOPITT and first results related to detection of enhanced CO over cities, *Atmos. Chem. Phys*. **7**: 2399-2411.

Buchwitz, M., O. Schneising, J. P. Burrows, H. Bovensmann, M. Reuter, and J. Notholt, First direct observation of the atmospheric CO_2 year-to-year increase from space, 2007b, *Atmos. Chem. Phys*. **7**: 4249-4256.

Burrows, J. P., M. Weber, M. Buchwitz, V.V. Rozanov, A. Ladstätter-Weissenmayer, A. Richter, R. de Beek, R. Hoogen, K. Bramstedt, K.-U. Eichmann, M. Eisinger, and D. Perner, 1999, The Global Ozone Monitoring Experiment (GOME): Mission concept and first scientific results, *J. Atm. Sciences*, 56, 151-175.

Chandrasekhar, S., 1960, *Radiative transfer*, Dover, N. Y.

Coldewey-Egbers, M., M. Weber, L. N. Lamsal, R. de Beek, M. Buchwitz, and J. P. Burrows, 2005, Total ozone retrieval from GOME UV spectral data using the weighting function DOAS approach, *Atmos. Chem. Phys*. **5**: 5015-5025.

de Laat, A. T. J., A. M. S. Gloudemans, H. Schrijver, M. M. P. van den Broek, J. F. Meirink, I. Aben, M. and Krol, 2006, Quantitative analysis of SCIAMACHY carbon monoxide total column measurements, *Geophys. Res. Lett.* **33**, L07807, doi:10.1029/2005GL025530.

Dils, B., M. De Maziere, T. Blumenstock, F. Hase, I. Kramer, F. Mahieu, P. Demoulin, P. Duchatelet, J. Mellqvist, A. Strandberg, M. Buchwitz, I. Khlystova, O. Schneising, V. Velazco, J. Notholt, R. Sussmann, and W. Stremme, 2006, Validation of WFM-DOAS v0.6 CO and v1.0 CH_4 scientific products using European ground-based FTIR measurements, proceedings of the Third Workshop on the Atmospheric Chemistry Validation of ENVISAT (ACVE-3), 4-7 Dec. 2006, ESA/ESRIN, Frascati, Italy, ESA Publications Division Special Publication SP-642 (CD).

Eisinger, M., and J. P. Burrows, 1998, Tropospheric sulfur dioxide observed by the ERS-2 GOME instrument, *Geophys. Res. Lett.* **25**: 4177-4180.

Eskes, H. J., R. J. van der A, E. J. Brinksma, J. P. Veefkind, J. F. de Haan, and P. J. M. Valks, 2005, Retrieval and validation of ozone columns derived from measurements of SCIAMACHY on Envisat, *Atmos. Chem. Phys. Discuss.,* **5**, 4429--4475.

Frankenberg, C., U. Platt, and T. Wagner, Retrieval of CO from SCIAMACHY onboard ENVISAT, 2005a, Detection of strongly polluted areas and seasonal patterns in global CO abundances, *Atmos. Chem. Phys*. **5**: 1639-1644.

Frankenberg, C., J. F. Meirink, M. van Weele, U. Platt, and T. Wagner, 2005b, Assessing methane emissions from global spaceborne observations, *Science*, **308**: 1010-1014.

Frankenberg, C., J. F. Meirink, P. Bergamaschi, A. P. H. Goede, M. Heimann, S. Körner, U. Platt, M. van Weele, and T. Wagner, 2006, Satellite chartography of atmospheric methane from SCIAMACHY onboard ENVISAT: Analysis of the years 2003 and 2004, *J. Geophys. Res.* **111**, D07303, doi:10.1029/2005JD006235.

Gloudemans, A. M. S., M. C. Krol, J. F. Meirink, A. J. T. de Laat, R. van der Werf, H. Schrijver, M. M. P. van den Broek, and I. Aben, 2006, Evidence for long-range transport of carbon monoxide in the southern hemisphere from SCIAMACHY observations,*Geophys. Res. Lett*. **33**, L16807, doi:10.1029/2006GL026804.

Gottwald, M., H. Bovensmann, G. Lichtenberg, et al., 2006, *SCIAMACHY: Monitoring the changing Earth's atmosphere*, Oberpfaffenhofen: DLR.

Kokhanovsky, A. A., W. von Hoyningen-Huene, and J. P. Burrows, 2006, Atmospheric aerosol load as derived from space, *Atmos. Res*., **81**: 176-185.

Kokhanovsky, A. A., B. Mayer, V. V. Rozanov, K. Wapler, L. N. Lamsal, M. Weber, J.

P. Burrows, and U. Schumann, 2007a, Satellite ozone retrieval under broken cloud conditions: an error analysis based on Monte Carlo simulations, *IEEE Trans. Geosci. Rem. Sens.*, **45**: 187-194.

Kokhanovsky, A. A., B. Mayer, V. V. Rozanov, K. Wapler, J. P. Burrows, and U. Schumann, 2007b, The influence of broken cloudiness on cloud top height retrievals using nadir observations of backscattered solar radiation in the oxygen A-band, *J. Quant. Spectr. Rad. Transfer*, **103**: 460-477.

Kokhanovsky, A. A., K. Bramstedt, W. von Hoyningen-Huene, and J. P. Burrows, 2007c, The intercomparison of top-of-atmosphere reflectivity measured by MERIS and SCIAMACHY in the spectral range of 443–865 nm**,** *Trans. Geosciences and Remote Sensing, Letters, IEEE***,** **4**: 293 – 296.

Kokhanovsky, A. A., M. Vountas, V. V. Rozanov, W. Lotz, H. Bovensmann, and J. P. Burrows, 2007d, Global cloud top height distribution and thermodynamic phase distributions as obtained by SCIAMACHY on ENVISAT, *Int. J. Remote Sens.* **28**: 4499-4507.

Kokhanovsky, A. A., F.-M. Breon, A. Cacciari, et al., 2007e, Aerosol remote sensing over land: a comparison of satellite retrievals using different algorithms and instruments, *Atmos. Res.* **85**: 372-394.

Krueger, A. J., L. S. Walter, P. K. Bhartia, C. C. Schnetzler, N. A. Krotkov, I. Sprod, and G. J. S. Bluth, 1995, Volcanic sulfur dioxide measurements from the total ozone mapping spectrometer instruments, *J. Geophys. Res.* **D100**: 14057-14076.

Ladstätter-Weißenmayer, A., J. Meyer-Arnek, A. Schlemm, and J. P. Burrows, 2004, Influence of stratospheric airmasses on tropospheric vertical O_3 columns based on GOME (Global Ozone Monitoring Experiment) measurements and backtrajectory calculation over the Pacific, *Atmos. Chem. Phys.* **4**: 903–909.

Ladstätter-Weißenmayer, A., M. Kanakidou, J. Meyer-Arnek, E. V. Dermitzaki, A. Richter, M. Vrekoussis, F. Wittrock, and J.P. Burrows, 2007, Pollution events over the East Mediterranean: Synergistic use of GOME, ground based and sonde observations and models, *Atmospheric Environment*, in press.

Lamsal, L. N., M. Weber, G. Labow, and J.P. Burrows, 2007, Influence of ozone and temperature climatology on the accuracy of satellite total ozone retrieval, *J. Geophys. Res.*,**112**, , doi:10.1029/2005JD006865.

Leue, C., M. Wenig, T. Wagner, U. Platt, and B. Jähne, 2001, Quantitative analysis of NO_x emissions from GOME satellite image sequences, *J. Geophys. Res.* **106**: 5493-5505.

Martin, R. V., D. J. Jacob, K. Chance, T. P. Kurosu, P. I. Palmer and M. J. Evans, 2003, Global inventory of nitrogen oxide emissions constrained by space-based observations of NO_2 columns, *J. Geophys. Res*. **108**, 4537-4548.

Noël, S., M. Buchwitz, H. Bovensmann, R. Hoogen, and J. P. Burrows, 1999,
Atmospheric water vapor amounts retrieved from GOME satellite data, *Geophys. Res. Lett.* 26, 1841-1844.

Noël, S., M. Buchwitz, and J. P. Burrows, First retrieval of global water vapour column amounts from SCIAMACHY measurements, 2004, *Atmos. Chem. Phys.* **4**: 111-125.

Noël, S., M. Buchwitz, H. Bovensmann, and J. P. Burrows, 2005, Validation of SCIAMACHY AMC-DOAS water vapour columns, *Atmos. Chem. Phys.,* **5**: 1835-1841.

Noël, S., S. Mieruch, H. Bovensmann, and J. P. Burrows, 2007, A combined GOME and SCIAMACHY global water vapour data set, *Proc. ENVISAT Symposium, Montreux, Switzerland, 23–27 April 2007* (ESA SP-636).

Oltmans, S. J.II, I. E. Galbally, E.-G. Brunke, C. P. Meyer, J. A. Lathrop, B. J. Johnson, D. S. Shadwick, E. Cuevas, F. J. Schmidlin, D. W. Tarasick, H. Claude, J. B. Kerr, O. Uchino, V. Mohnen, 1998, Trends of ozone in the troposphere, *Geophys. Res. Lett.* **25**: 139–142.

Mieruch, S., S. Noël, H. Bovensmann, and J. P. Burrows, 2007, Analysis of global water vapour trends from satellite measurements in the visible spectral range, *Atmos. Chem. Phys. Discuss.* 7: 11761–11796.

Platt, U., 1994, Differential optical absorption spectroscopy (DOAS), in *Air monitoring by spectroscopic techniques*, Chem. Anal. Ser., 127, edited by M. W. Sigist, N. Y.: John Wiley.

Platt, U., and S. Stutz, 2008, *Differential Optical Absorption Spectroscopy:Principles and Applications*, Springer, Berlin.

Remer, L. A., Y. J. Kaufman, D. Tanré, S. Mattoo, D. A. Chu, J. V. Martins, R-R. Li, C. Ichoku, R. C. Levy, R. G. Kleidman, T. F. Eck, E. Vermote, and B. N. Holben, 2005, The MODIS aerosol algorithm, products and validation, *J. of Atmos. Sci.* **62**: 947-973.

Richter, A. and J. P. Burrows, 2002, Retrieval of tropospheric NO_2 from GOME measurements, *Adv. Space Res.* **29**: 16673-1683.

Richter, A., V. Eyring, J. P. Burrows, H. Bovensmann, A. Lauer, B. Sierk, and P. J. Crutzen, 2004, Satellite measurements of NO_2 from international shipping emissions, *Geophys. Res. Lett.*, **31**, L23110, doi:10.1029/2004GL020822.

Richter, A., J. P. Burrows, H. Nüß, C., Granier, and U. Niemeier, 2005, Increase in tropospheric nitrogen dioxide over China observed from space, *Nature* **437**: 129-132.

Rozanov, V. V., T. Kurosu, and J.P. Burrows, 1998, Retrieval of atmospheric

constituents in the uv-visible: a new quasi-analytical approach for the calculation of weighting functions, *J. Quant. Spectr. Rad. Trans.* **60**: 277-299.

Sierk, B., A. Richter, A. A. Rozanov, C. von Savigny, A. M. Schmoltner, M. Buchwitz, H. Bovensmann, and J. P. Burrows, 2006, Retrieval and monitoring of atmospheric trace gas concentrations in nadir and limb geometry using the space-borne SCIAMACHY instrument, *Environmental Monitoring and Assessment*, doi: 10.1007/s10661-005-9049-9.

van de Hulst, H. C., 1957, *Light Scattering by Small Particles*, Wiley&Sons, N. Y.

van Diedenhoven, B., 2007, *Satellite remote sensing of cloud properties in support of tropospheric trace gas retrievals*, PhD thesis, Free University, Amsterdam.

van Roozendael, M., D. Loyola, R. Spurr, D. Balis, J.-C. Lambert, Y. Livschitz, P. Valks, T. Ruppert, P. Kenter, C. Fayt, and C. Zehner, 2006, Ten years of GOME/ERS-2 total ozone data: The new GOME data processor (GDP) version 4: 1. Algorithm description, *J. Geophys. Res.*, **111**, doi:10.1029/2005JD006375.

von Hoyningen-Huene, W., M. Freitag, and J. P. Burrows, 2003, Retrieval of aerosol optical thickness over land surfaces from top-of-atmosphere radiance, *J. Geophys. Res*. **108**, doi: 10.1029/2001JD002018.

von Hoyningen-Huene, W., A. A. Kokhanovsky, J. P. Burrows, 2007, Retrieval of particulate matter from MERIS observations, in *Advanced Environmental Monitoring,* ed. by U. Platt and J. Kim, Berlin: Springer, in press.

von Savigny, C., V., A. A. Rozanov, H. Bovensmann, et al., 2005, The ozone hole break-up in September 2002 as seen by SCIAMACHY on Envisat, *J. Atmos. Sci.* **62**: 721–734.

Weber, M., L. N. Lamsal, M. Coldewey-Egbers, K. Bramstedt, and J. P. Burrows, 2005, Pole-to-pole validation of GOME WFDOAS total ozone with ground based data, *Atmos. Chem. Phys*. **5**: 1341-1355.

Zhang, Q. , D. G. Streets, K. He, et al., 2007, NO_x emission trends for China, 1995-2004: The view from the ground and the view from space, *J. Geophys. Res.,* in press.